



A Hydroxylated Tetracationic Viologen based on Dimethylaminoethanol as a Negolyte for Aqueous Flow Batteries

Carlo Caianiello,^[a] Luis F. Arenas,^[b, c] Thomas Turek,^[b, c] and René Wilhelm^{*[a]}

A tetracationic viologen based on dimethylaminoethanol is reported as a novel negolyte for aqueous-organic flow batteries. The compound (1,1'-bis(3-((2-hydroxyethyl)dimethylammonio)propyl)-[4,4'-bipyridine]-1,1'-dium tetrachloride), termed $[(DMAE-Pr)_2-Vi]Cl_4$, was prepared by replacing the trimethylammonium groups of a former analogue for dimethylaminoethanol derivatives as permanently charged moieties, improving its solubility and modifying its electronic structure,

as revealed by DFT calculations. Its electrochemical properties and diffusion coefficient were investigated by voltammetry and DOSY. The battery concept was demonstrated by pairing $[(DMAE-Pr)_2-Vi]Cl_4$ with a TEMPOL posolyte using a low-cost anion exchange membrane and a neutral-pH supporting electrolyte. $[(DMAE-Pr)_2-Vi]Cl_4$ has great potential for enhancing energy density in viologen flow batteries.

Introduction

Flow batteries (FBs) are scalable technology capable of long duration discharge and service mode flexibility,^[1,2] delivering an option for the stationary storage of renewable energy.^[3] Aqueous FBs based on redox-active organic molecules (OFBs) could circumvent cost and supply limitations experienced by other types of batteries.^[4,5] Organic molecules can be synthesized from abundant commodities and be tailored to improve solubility, calendar stability, redox potential and reaction kinetics.^[6] One of the challenges in this field is the development of long-lasting molecules for high-capacity electrolytes.^[7,8]

Viologens, trivial name for 4,4'-bipyridinium derivatives, are of interest in electrochromic devices, molecular machines and batteries.^[9,10] They can be water-soluble and constitute a family of redox-active compounds exhibiting three redox states, Vi^{2+} (dicationic), Vi^+ (radical cation),^[11] and Vi^0 (neutral).^[12] Current interest arises from their electron-accepting capability and the

fact that substituents on the nitrogen atoms can be easily tuned, mainly via straightforward S_N2 reactions.^[9] Substituent groups are of crucial importance, since they control the electrochemical and solvation properties,^[13] although the latter depends on the counter-anion in solution too.^[9] Given their redox potentials, viologens are suited for the negative half-cell of OFBs. Methyl viologen (MV), or paraquat, is the simplest viologen and an industrial herbicide, being studied due to its electrochemical properties, water solubility (2.5 M)^[14] and direct synthesis.^[15] However, MV and viologens in general are vulnerable to decomposition in solution through a bimolecular mechanism.^[16] Moreover, their permeability through ion exchange membranes contributes to capacity loss.^[16,17]

In order to overcome these problems, "molecular engineering" strategies have come in place to tune relevant properties through the choice of N-substituents.^[15] Pendant charged groups are particularly promising, specifically sulfonate,^[18] phosphonate^[17] and quaternary ammonium.^[19] Among these, superior battery performance appears to result from tethering a positively charged group, e.g., trimethylammonium moiety, to the 4,4'-bipyridine core; the obtained tetracationic viologens theoretically allow the storage of two electrons per molecule while retaining two permanently charged moieties that assure solubility, Coulombic repulsion (radical cations), and low membrane permeability.^[16] Despite the performance obtained when storing one electron in couple with various posolytes,^[16,19] the second electron accelerates molecular degradation. While the stability of the radical tri-cation has been proved,^[20,21] the radical dication (i.e., quinoid-like structure for the bipyridine) remains unstable.^[20]

Aiming to advance the molecular engineering of viologens, a new, hydroxylated tetracationic variant bearing two ethanolamine residues is here presented (Figure 1a). The main structure was inspired by a previously reported analogue (BTMAP-Vi, Figure 2a).^[19] A different permanently charged moiety was selected, switching from the trimethylammonium

[a] C. Caianiello, Prof. Dr. R. Wilhelm
Institute of Organic Chemistry
Clausthal University of Technology
Leibnizstraße 6, 38678 Clausthal-Zellerfeld, Germany
E-mail: rene.wilhelm@tu-clausthal.de

[b] Dr. L. F. Arenas, Prof. Dr. T. Turek
Institute of Chemical and Electrochemical Process Engineering
Clausthal University of Technology
Leibnizstraße 17, 38678 Clausthal-Zellerfeld, Germany

[c] Dr. L. F. Arenas, Prof. Dr. T. Turek
Research Center for Energy Storage Technologies
Clausthal University of Technology
Am Stollen 19 A, 38640 Goslar, Germany

Supporting information for this article is available on the WWW under <https://doi.org/10.1002/batt.202200355>

An invited contribution to a Special Collection on Organic Batteries

© 2022 The Authors. *Batteries & Supercaps* published by Wiley-VCH GmbH. This is an open access article under the terms of the Creative Commons Attribution Non-Commercial License, which permits use, distribution and reproduction in any medium, provided the original work is properly cited and is not used for commercial purposes.

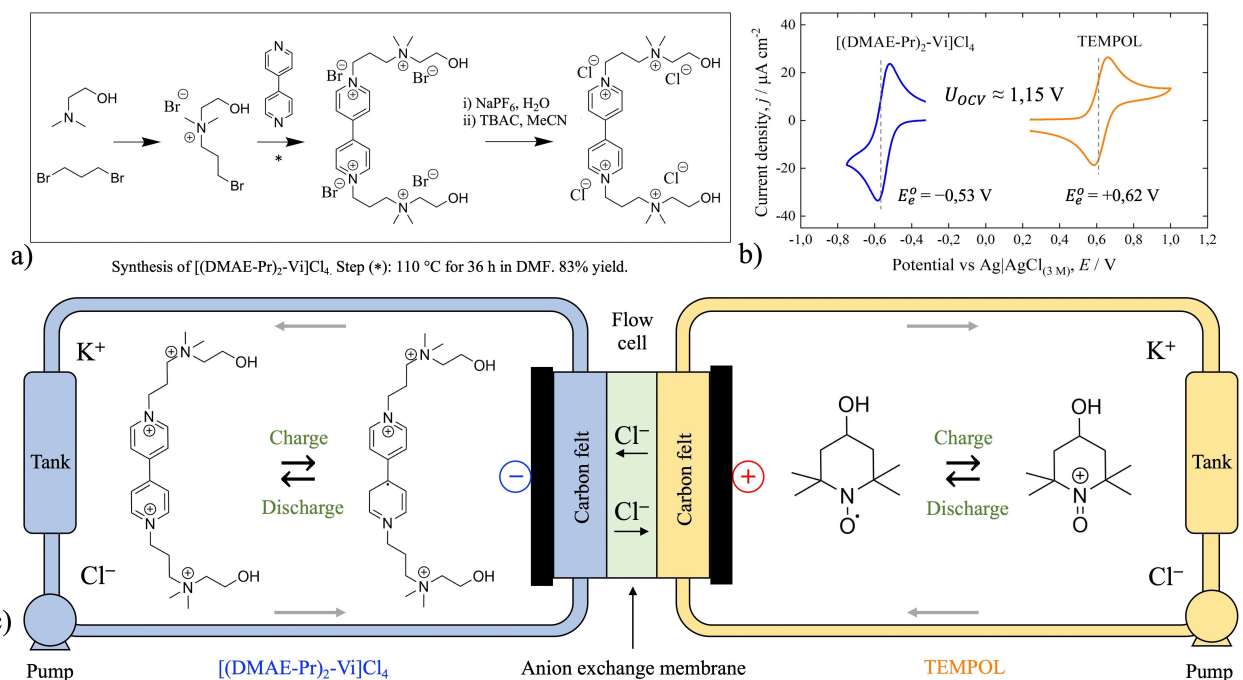


Figure 1. Flow battery based on a tetracationic hydroxylated viologen derivative negolyte: $[(\text{DMAE-Pr})_2\text{-Vi}]Cl_4$. a) Synthetic route. b) Cyclic voltammograms and relevant potentials for $[(\text{DMAE-Pr})_2\text{-Vi}]Cl_4$ and TEMPOL in 0.1 M KCl (100 mV s^{-1}). c) Schematic representation of the aqueous-organic flow battery.

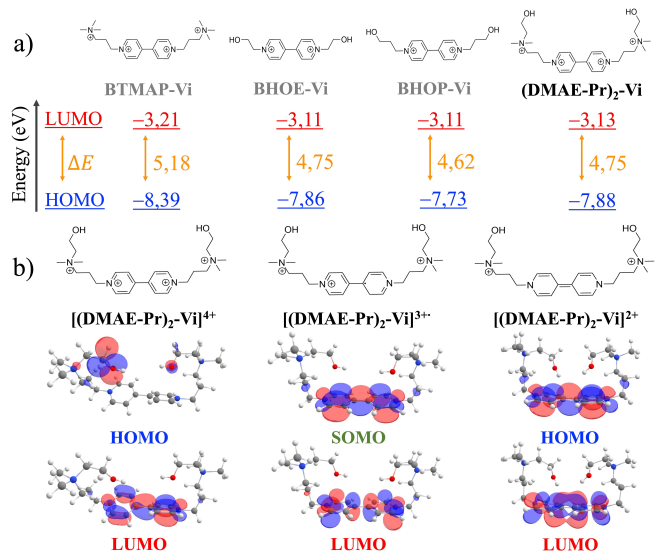


Figure 2. a) HOMO-LUMO levels (DFT recalculated with parameters as for $(\text{DMAE-Pr})_2\text{-Vi}$) for BTMAP-Vi, BHOE-Vi, BHOP-Vi (Ref. [22]) and $(\text{DMAE-Pr})_2\text{-Vi}$; b) Optimized DFT structures for $(\text{DMAE-Pr})_2\text{-Vi}$ in its three redox states, frontier HOMO/SOMO and LUMO orbitals.

group to a dimethylaminoethanol (DMAE) derivative. DMAE is a bifunctional compound, containing both hydroxyl and tertiary amine groups. Indeed, the addition of hydroxyl-containing substituents to a series of bis-cationic viologens lead to enhanced water-solubility and hydrophilicity.^[22] It was speculated that the same outcome could be obtained with tetracationic viologens.

This work presents the feasibility of the proposed synthetic approach and the characterization of its product through

different techniques. The resulting compound is denoted as $[(\text{DMAE-Pr})_2\text{-Vi}]Cl_4$, or $(1,1'\text{-bis}(3\text{-(2-hydroxyethyl)dimethylammonio})\text{propyl})\text{-}[4,4'\text{-bipyridine}]\text{-}1,1'\text{-diium tetrachloride}$. Its application in a new viologen-based negolyte for aqueous OFBs is then demonstrated in a flow battery along a 4-OH-TEMPO (TEMPOL) posolyte and an anion exchange membrane by evaluating cell performance over various operational conditions and capacity retention under charge-discharge operation.

Results and Discussion

The synthetic pathway consists of two successive Menshutkin reactions (S_N2) with high yield and product purity without requiring further purification procedures. The first step is the alkylation of DMAE using an excess of 1,3-dibromopropane to avoid any bis-alkylation (Figure 1a). The second and final step is the alkylation of the 4,4'-bipyridine with the intermediate obtained in the first step. This route was easily scaled-up to 8 g (83% yield for the second step). The bromine salt was characterized by NMR and HR-ESIMS (Figures S1–S5). In order to avoid electrochemical or membrane reactions with Br^- , this counteranion was exchanged to Cl^- by two consecutive metatheses; an ion exchange column could be used alternatively, e.g., Ref. [23]. No differences were found in the NMR spectra or voltammetry of the two salts (Figures S7, S8 and S12). The solubility of $[(\text{DMAE-Pr})_2\text{-Vi}]Cl_4$ was then measured by UV-Vis spectroscopy (Figure S9 and S10). The value for water is $2.7 \text{ M} (\pm 0.3)$ at 22°C , making $[(\text{DMAE-Pr})_2\text{-Vi}]Cl_4$, to the best of our knowledge, the tetracationic viologen with the highest

water solubility ever reported. The earlier analogue (having two trimethylammonium groups) has a reported solubility ranging from 1.6 M (Br^-) to 2.0 M (Cl^-) in water.^[16,19] Considering the value for Cl^- , it can be asserted that the addition of two OH-groups, increased the solubility in water by approximately 35%. Dex-Vi, which adds two hydroxyl groups to the BTMAP-Vi structure, has a similar solubility of 2.0 M (Cl^-) in water.^[24] Given the lower molecular weight of Dex-Vi, the solubility of $[(\text{DMAE-Pr})_2\text{-Vi}] \text{Cl}_4$ suggests that the position of its OH-groups at the end of the substituents, and not between other charged groups, plays a role in solvation, perhaps by enabling them to install hydrogen bonds.

Density functional theory (DFT) calculations were conducted to gain a deeper understanding on the effect of introducing hydroxyl groups on the electronic structure of $[(\text{DMAE-Pr})_2\text{-Vi}] \text{Cl}_4$, for details see Supporting Information. The calculated HOMO energy is -7.88 eV, while the LUMO energy is -3.13 eV, affording an energy gap of 4.75 eV. The calculations are in agreement with the trend of higher LUMO energy for hydroxylated viologens reported by Liu et al.^[22]

Indeed, the tetracationic viologen bearing two trimethylammonium groups (BTMAP-Vi) has a HOMO energy of -8.39 eV and a LUMO energy of -3.21 eV, i.e., a gap of 5.18 eV (Figure 2a); simple dicationic viologens bearing two ethanol (BHOE-Vi) or propanol (BHOP-Vi) moieties have a HOMO energy of -7.86 eV and -7.73 eV while the LUMO energy is -3.11 eV and -3.11 eV, respectively, leading to gaps of 4.75 eV and 4.62 eV.^[22]

An interesting observation can be made for the optimized ground state (Figure 2b) of the three redox states of $[(\text{DMAE-Pr})_2\text{-Vi}] \text{Cl}_4$. The oxygen atoms of the OH-groups are always pointing at the redox centers (i.e., the bipyridinium rings) of

$[(\text{DMAE-Pr})_2\text{-Vi}]^{4+}$ and $[(\text{DMAE-Pr})_2\text{-Vi}]^{3+}$, yet for the latter not directly to the center of each ring. A weak interaction between bipyridinium (especially the radical cation) and the oxygen atoms of the OH-groups has been recently proposed to explain the mitigated dimerization of ethyl viologen radical cation and α -cyclodextrin.^[25] Based on the DFT calculations, it can be speculated that a similar interaction could take place. However, it should be underlined that, in this case, there are two hydroxyl groups per viologen and the interaction would eventually be intramolecular, while when using the α -cyclodextrin there are numerous hydroxyl groups per viologen and the interaction is intermolecular. Remarkably, in the $[(\text{DMAE-Pr})_2\text{-Vi}]^{2+}$ structure the hydrogen atoms of the OH-groups are pointing to the newly formed double bond between the pyridine rings, indicating a hydrogen- π -interaction. However, this interaction is not strong enough to stabilize the fully reduced species in order to utilize the second reduction for the battery.

Cyclic voltammetry of $[(\text{DMAE-Pr})_2\text{-Vi}] \text{Cl}_4$ at low concentrations reveals that the formal redox potential for the $(\text{DMAE-Pr})_2\text{-Vi}^{4+}/(\text{DMAE-Pr})_2\text{-Vi}^{3+*}$ couple is -0.53 V vs $\text{Ag}/\text{AgCl}_{(3\text{ M})}$, while for the $(\text{DMAE-Pr})_2\text{-Vi}^{3+*}/(\text{DMAE-Pr})_2\text{-Vi}^{2+}$ couple is -0.89 V vs. $\text{Ag}/\text{AgCl}_{(3\text{ M})}$ (Figure 3a). Equivalent to -0.33 and -0.69 V vs. SHE, respectively, these values display a small positive shift compared to the non-hydroxylated analogue (-0.35 and -0.72 V vs. SHE, respectively).^[19] DFT calculation of the SOMO of $(\text{DMAE-Pr})_2\text{-Vi}^{3+*}$ was -4.17 eV, which corresponds to -0.33 V vs. SHE and is in very good agreement with the measured value (for more details see Supporting Information). This confirms that the main influence on the redox potential comes from the proximity of a strong electron-withdrawing group (ammonium salt) rather than the substituents on the

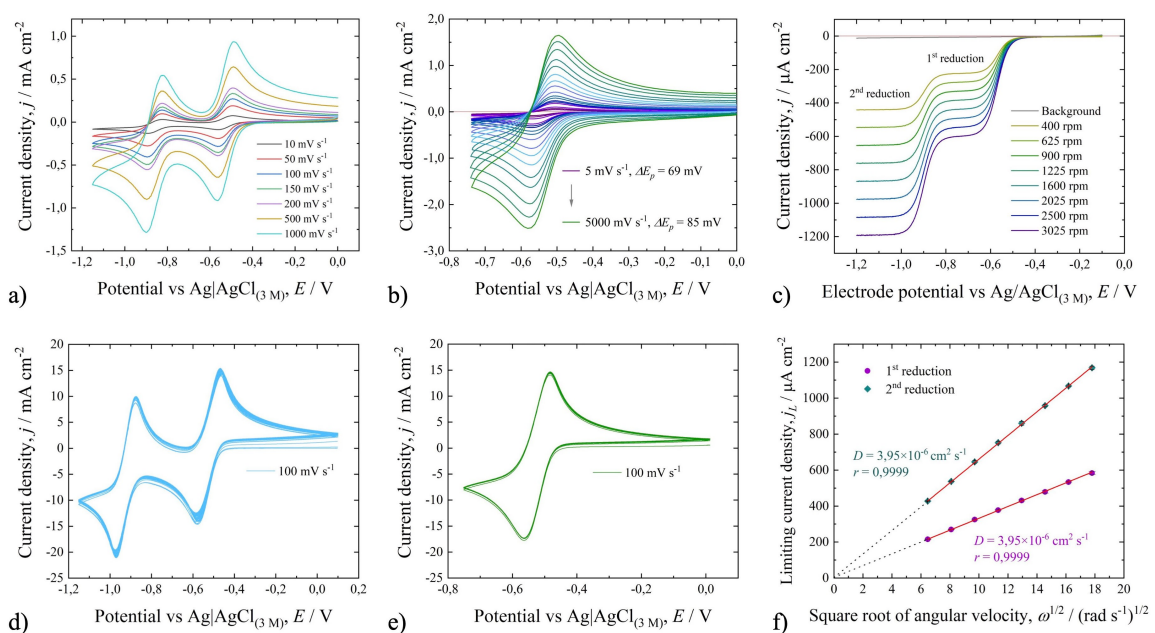


Figure 3. Electrochemical characterization of $[(\text{DMAE-Pr})_2\text{-Vi}] \text{Cl}_4$. Cyclic voltammetry at 2 mM in 0.1 M KCl: a) first and second reductions, b) first reduction; c) linear sweep voltammetry for both redox events at rotating disc electrode at 1 mM in 0.5 M KCl; extended cyclic voltammetry at 0.1 M in 1 M KCl, 200 scans: d) first and second reductions, e) first reduction; f) Levich plot for the determination of diffusion coefficients from the linear sweep voltammetry.

latter. The voltammograms for the first reduction (Figure 3b) display a remarkable electrochemical reversibility, with a peak separation of 85 mV at a scan rate of 5 V s^{-1} (Figure S13, Table S1), which renders the Koutecký-Levich method for determination of kinetic parameters inapplicable,^[26] and the Nicholson approach in need of ultramicroelectrodes.^[27] It can be cautiously suggested that the standard rate of $[(\text{DMAE-Pr})_2\text{-Vi}]Cl_4$ would likely fall in the same range of BTMAP-Vi ($k_s = 0.28 \text{ cm s}^{-1}$),^[27] but measurements with adequate techniques are nevertheless required to establish an accurate value. From an electrochemical engineering point of view, the voltammogram reversibility implies small overpotentials, hence access to greater energy efficiency (EE). Cyclic voltammograms were acquired at higher concentrations (0.1 M in 1 M KCl), performing 200 reduction-oxidation cycles at 100 mV s^{-1} as a preliminary assessment of the effect of concentration on the species stability.^[27] It was observed that loss of redox activity, as denoted by decreasing peak current densities, occurred when accessing the second reduction (Figure 3d) in contrast to the first reduction only (Figure 3e). As a result, flow battery operation was restricted to the first redox event.

At a rotating disc electrode, the limiting current for the second reduction is exactly twofold of the first reduction (Figure 3c), as in the case of MV in a non-aqueous solvent,^[28] suggesting an absence of comproportionation kinetics.^[29] Full diffusion control is confirmed by collapsing the voltammograms into a single curve by normalizing for limiting current (Figure S14). Identical diffusion coefficients of $D = 3.92 \times 10^{-6} \text{ cm}^2 \text{s}^{-1}$ in 0.5 M KCl were determined for $[(\text{DMAE-Pr})_2\text{-Vi}]Cl_4$

from its two reduction events (1e^- , 2e^-) in a Levich plot (Figure 3f), with linear relationships extrapolating to the origin. This value is consistent with a Randles-Ševčík analysis for the same compound in 0.1 M KCl ($4.02 \times 10^{-6} \text{ cm}^2 \text{s}^{-1}$) (see Experimental Section). In contrast, for the non-hydroxylated analogue BTMAP-Vi, $D = 3.3 \times 10^{-6} \text{ cm}^2 \text{s}^{-1}$ in 0.5 M NaCl.^[16] For MV, $D = 4.4 \times 10^{-6} \text{ cm}^2 \text{s}^{-1}$ in 0.5 M KCl,^[30] due to its smaller molecular mass. The diffusion coefficient of $[(\text{DMAE-Pr})_2\text{-Vi}]Cl_4$ in the supporting electrolyte of the flow battery (1 M KCl) was estimated by DOSY to be $3.2 \times 10^{-6} \text{ cm}^2 \text{s}^{-1}$ (Figure S6). Similar DOSY results were reported for new conjugated viologens.^[31] These findings imply that the molecular mass of $[(\text{DMAE-Pr})_2\text{-Vi}]Cl_4$ has no detrimental effect on its diffusivity when compared to BTMAP-Vi.

A flow battery was then set using 0.1 M $[(\text{DMAE-Pr})_2\text{-Vi}]Cl_4$ in 1 M KCl as the capacity-limiting negolyte, 0.1 M TEMPOL in 1 M KCl as the non-limiting posolyte ($2 \times$ volumetric excess) and a low-cost,^[32] anion exchange membrane (Cl^-), Fumasep® FAS-30 (Fumatech BWT GmbH). The flow battery was fitted with oxygen-impermeable gaskets and tubes and maintained the electrolytes under a positive pressure of nitrogen. Charge-discharge operation was first performed galvanostatically at different current densities with voltage cut-off values of 0.6 and 1.4 V. The maximum accessible capacity was 94% at 20 mA cm^{-2} (Figure 4a). When comparing the efficiencies shown in Figure 4b to similar flow systems,^[19,33] this work affords higher EE, i.e., 78% at 60 mA cm^{-2} vs. $\approx 60\%$ for Ref. [19] and Supporting Information from Ref. [34]. These results also confirm that the FAS-30 membrane can be an

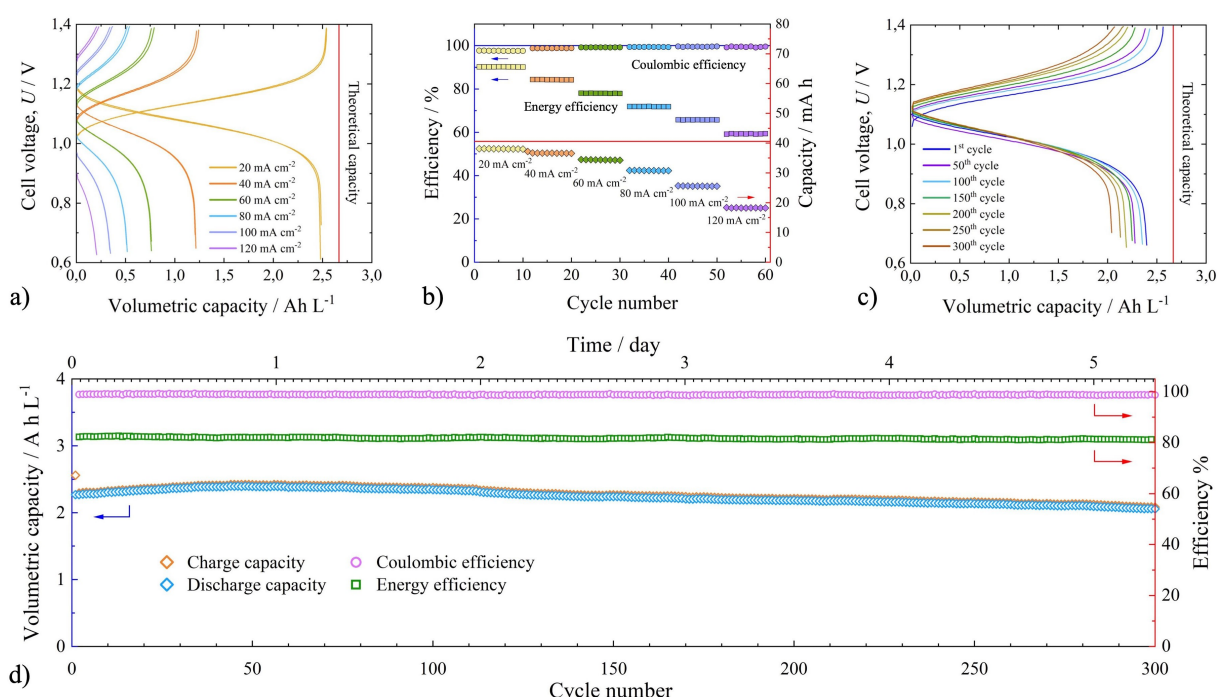


Figure 4. A $[(\text{DMAE-Pr})_2\text{-Vi}]Cl_4/\text{TEMPOL}$ flow battery proof of concept with both redox couples at a concentration of 0.1 M in 1 M KCl. Effect of current density on: a) Accessible volumetric capacity (1st, 10th cycle for each value); b) Coulombic and energy efficiencies and accessible capacity (10 cycles per value); demonstration of cell cycling at 40 mA cm^{-2} ; c) voltage and volumetric capacity vs. cycle; d) volumetric capacity and coulombic and energy efficiencies vs time and cycle.

alternative to Nafion[®]^[32] and Slemion[®] DSV in OFBs.^[16,22,35] For comparison, the DSV type provided an EE of 79% at 60 mA cm^{-2} for 0.5 M of MV in 2 M KCl.^[30] Nearly the same EE is found in Figure 4b, but for 0.1 M of electroactive substance and 1 M of supporting electrolyte.

Flow battery operation was demonstrated under a galvanostatic charge-discharge regime for 300 cycles (127 h) at a typical current density of 40 mA cm^{-2} . During this period, the accessible volumetric capacity decreased from 84% to 76% (Figure 4c) and $\approx 8\%$ of the initial accessible capacity was lost, with an average capacity retention of 99.96% and an average EE of 81.1%. A jump in the accessed capacity was observed between the 1st and 2nd cycle, going from 97% to 84% of the theoretical value. Such loss cannot be explained by decomposition or presence of oxygen. The accessible capacity was thus defined from the second cycle in agreement with the literature.^[16] This capacity jump can be attributed to mass transport resistance,^[17] and to a resistance change resulting from the time-dependent uptake, and possible reaction, of the redox couples within the membrane during the 1st cycle.^[34] An increase in apparent capacity occurs between the 1st and 50th cycle (Figure 4d), liable to a rising membrane conductivity and the same membrane processes. The capacity fade rate at quasi steady state was 3.1% per day (0.054% per cycle), as taken from the slope between the 150th and 300th cycle (8.2% loss). In contrast, a flow battery using a related [(Me)(NPr)V]Cl₃ viologen^[19] showed a capacity fade rate of 0.04% per cycle ($\approx 13\%$ over 300 cycles) when accessing the second reduction. A system with a π -conjugated viologen [(NPr)₂TTz]Cl₄^[33] showed a similar capacity fade rate of 0.03% per cycle ($\approx 10\%$ over 300 cycles) at 40 mA cm^{-2} , accessing the second reduction too. And a flow battery with an unsymmetrical viologen, reported a capacity fade of 0.022% per cycle (4.4% over 200 cycles) in 2 M NaCl at 30 mA cm^{-2} .^[36] However, cell cycle duration and calendar capacity fade rate were not reported for the above cases. The battery in this work sustained higher cycle numbers than the ones in Ref. [19], Ref. [33], Ref. [36], perhaps by not accessing the unstable second reduction, noting that current density is lower than Ref. [19] (i.e., 40 vs. 60 mA cm^{-2}).

The calendar capacity fade rate of 3.1% per day is typical in freestanding, low-volume flow systems, despite the supply of nitrogen and the use of seemingly hermetic materials.^[37] Such fade rate is about twice that of MV in a glovebox.^[20] Further work is required to define a standard calendar capacity fade rate for [(DMAE-Pr)₂-Vi]Cl₄ under potentiostatic control in a glovebox in order to carry out firm comparisons of molecular stability.^[20] Enhanced capacity retention and prolonged cycling can be achieved for the full cell in the same way. Additional improvements could result from replacing the nitroxyl-radical posolyte by a ferrocene derivative,^[8] such as (ferrocenylmethyl)trimethylammonium chloride.^[38]

Indeed, TEMPOL is readily available but it is known to be unstable upon cycling and to have a significant membrane permeability.^[39] This was confirmed in our system by subjecting both electrolytes to cyclic voltammetry after the end of the galvanostatic cell cycling. The peaks corresponding to TEMPOL are clearly present in the spent negolyte (Figure 5a). On the

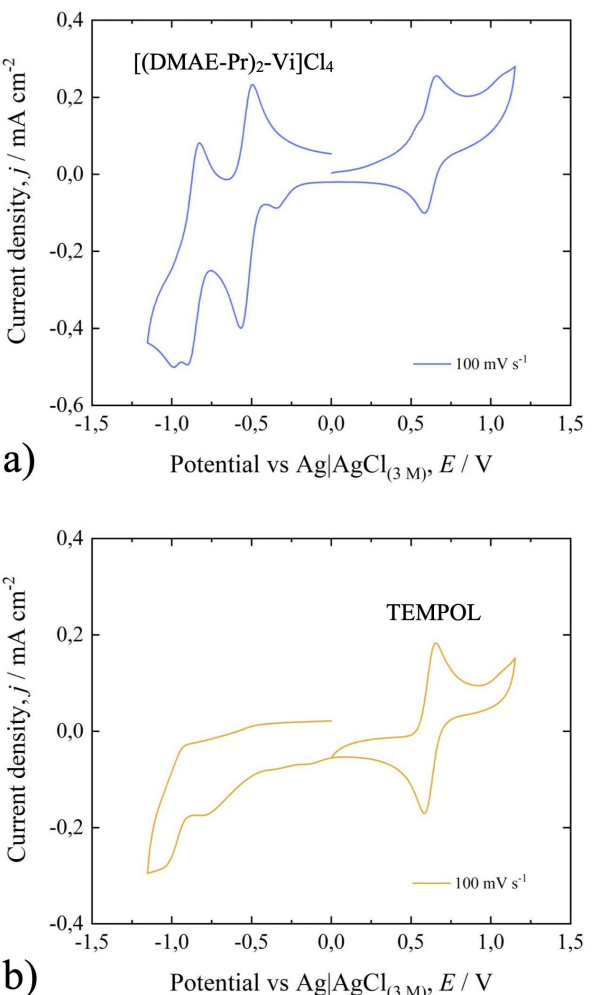


Figure 5. Post-mortem cyclic voltammograms for the spent [(DMAE-Pr)₂-Vi]Cl₄/TEMPOL electrolytes following 300 galvanostatic cycles at 40 mA cm^{-2} . a) [(DMAE-Pr)₂-Vi]Cl₄ negolyte. b) TEMPOL posolyte.

other hand, crossover of the viologen into the posolyte (Figure 5b) might have occurred only for its degradation product, as suggested by the peak reduction potentials corresponding to the dealkylated dicationic species; see below. These observations indicate that the crossover of redox species, mainly from the posolyte to the negolyte, plays an important role in capacity loss and can be addressed, to some extent, by using more selective membranes. Furthermore, the *post-mortem* cyclic voltammetry provides insight into the stability of the redox species. Incipient degradation of [(DMAE-Pr)₂-Vi]Cl₄ in the negolyte is shown by the formation of a small peak preceding the first reduction and a distorted reduction peak for the second reduction (Figure 5a). The latter is likely the viologen analogue with only one substituent, which should possess a lower reduction potential according to the literature ($\approx -1.0 \text{ V}$ vs. Ag/AgCl).^[40] The pH of the negolyte was ≈ 12 after the experiment, in agreement with the release of hydroxide ions during the oxidation of the viologen radical cation by molecular oxygen and its subsequent dealkylation.^[16] In the posolyte, the curves corresponding to TEMPOL remain un-

changed (Figure 5b), but the reduction peak at ≈ -0.75 V vs. Ag/AgCl can be ascribed to the reduction of the TEMPOL radical.^[41] A reduction peak at ≈ -1.0 V vs. Ag/AgCl not accompanied by an oxidation peak is close to the potential for the dealkylated viologen and might indicate that the viologen becomes also electrochemically inactive by protonation following crossover.^[16] This is expected, as the posolyte becomes acidic via TEMPOL degradation,^[42] confirmed here by the final pH the solution, which was ≈ 2 . No precipitates were observed in the electrolytes after the duration of the charge-discharge test. Regarding the viscosity of $[(\text{DMAE-Pr})_2\text{-Vi}]\text{Cl}_4$, no change in the initial value of a discharged battery negolyte (1.01 cSt) could be measured after charging the solution. This is in agreement with recent work with Dex-Vi, which shows that the viscosity of tetracationic viologens is manageable at practical concentrations,^[24] in contrast to organic molecules suffering from excessive viscosity due to undesired oligomerization.^[43]

The need for battery performance and capacity retention evaluations using concentrated solutions of $[(\text{DMAE-Pr})_2\text{-Vi}]\text{Cl}_4$ is recognized. Under these conditions, intermolecular interactions will result in differences in viscosity, diffusion coefficient, conductivity, electrode kinetics and degradation rates dependent on molecular aggregation mechanisms in respect to relatively diluted conditions.^[44] The further implementation of the proposed negolyte will need to consider trade-offs among the above mentioned properties and the accessible volumetric capacity in order to provide an assessment of technological potential.

Conclusion

A new hydroxylated tetracationic viologen has been reported, proving the suitability of dimethylaminoethanol as a hydrophilic moiety for viologen functionalization. The addition of OH-groups alters the electronic structure of the viologen and increases its solubility and latent electrolyte energy density. The compound $[(\text{DMAE-Pr})_2\text{-Vi}]\text{Cl}_4$ displays electrochemical reversibility and reasonable stability when the first electron is accessed.

Its feasibility in aqueous-organic flow batteries was demonstrated as a negolyte along the nitroxyl-radical TEMPOL as posolyte, affording an open circuit cell voltage of 1.15 V and an EE of 81% at 40 mA cm⁻². It has also been shown that the FAS-30 electrodialysis membrane is compatible with these redox-active organic compounds although its selectivity is deficient for this system. Degradation of $[(\text{DMAE-Pr})_2\text{-Vi}]\text{Cl}_4$ and battery capacity loss take place through known mechanisms and stability could be gained mainly by maintaining a neutral pH.^[42] Future work will focus on extending capacity retention and implementing a stable ferrocene-based posolyte.

Experimental Section

All substances were purchased from TCI Chemicals, Fluka or BLDpharm, stored under nitrogen when required and used as

received. Experiments were performed under a nitrogen atmosphere, unless otherwise stated. Deionized water with a conductivity of 18.2 MΩ cm was used in the preparation of the solutions. NMR data were collected with a Bruker spectrometer, either an AVANCE 400 MHz or an AVANCE III 600 MHz. Mass spectra (HRESI-MS) were acquired in an Agilent LC/MSD-System Serie HP 1100 (API-ES) spectrometer. IR spectra were recorded on a Bruker Alpha FT-IR spectrometer (platinum ATR). Decomposition point was measured on a DSC 6 (Perkin Elmer) and a TG 209F1 (Netzsch) under nitrogen. UV-Vis spectra were recorded on a Jasco V-650 spectrophotometer using high precision cell (quartz Suprasil®) from HellmaAnalytics (10 mm light path).

Synthesis of

3-bromo-N-(2-hydroxyethyl)-N,N-dimethylpropan-1-aminium bromide

The procedure was modified from the literature.^[45] In a typical experiment, 2-dimethylaminoethanol (4.3 mL, 3.8 g, 43 mmol, 1 equiv.) was dissolved in acetone (45 mL) to yield a < 1 M solution. This solution was then added dropwise to a concentrated solution (≈ 2 M) of 1,3-dibromopropane (22 mL, 43 g, 210 mmol, 5 equiv.) in the same solvent (100 mL) in an ice-bath. Once the addition was concluded, the mixture was slowly allowed to reach room temperature and stirred for 24 h under air. The mixture was then quenched with diethyl ether to crush out a second crop of product and filtered using a glass frit. The white solid obtained was then dried under high vacuum (11.85 g, 40.72 mmol, 96% yield). ¹H NMR (D₂O): 2.40 ppm (m, 2H), 3.19 ppm (s, 3H), 3.56 ppm (m, 6H), 4.04 ppm (m, 2H). HR-ESIMS: m/z calc. for C₇H₁₇BrNO⁺ 210.0488, found 210.0497. The data are consistent with previous reports.^[45]

Synthesis of

1,1'-bis(3-((2-hydroxyethyl)dimethylammonio)propyl)-[4,4'-bipyridine]-1,1'-dium tetrabromide, $[(\text{DMAE-Pr})_2\text{-Vi}] \text{Br}_4$

3-Bromo-N-(2-hydroxyethyl)-N,N-dimethylpropan-1-aminium bromide (8.03 g, 27.60 mmol, 2.15 equiv.) was added in N,N-DMF (60 mL). 4,4'-Bipyridine (2.01 g, 12.84 mmol, 1 equiv.) was added to this mixture and the temperature was raised to 110 °C for 36 h under air (all the solids dissolved upon heating). A yellowish solid crushed out over time. The mixture was then filtered using a glass frit and the solid washed with hot DMF, acetonitrile and diethyl ether. The solid was then dried under high vacuum (7.87 g, 10.66 mmol, 83% yield). ¹H NMR (D₂O + TMSP-d₄): 2.75 ppm (m, 4H, bpy⁺-CH₂CH₂CH₂N⁺), 3.26 (s, 12H, -CH₃), 3.62 ppm (m, 4H, CH₂CH₂OH), 3.70 ppm (m, 4H, CH₂N⁺), 4.08 ppm (m, 4H, CH₂OH), 4.93 ppm (t, 4H, j = 7.5Hz, bpy⁺-CH₂), 8.7 ppm (d, 4H, j = 6.8Hz, -CHCHN⁺ bpy), 9.27 ppm (d, 4H, j = 6.8Hz, -CHCHN⁺ bpy). ¹³C NMR (D₂O + TMSP-d₄): 24.4 ppm (bpy⁺-CH₂CH₂CH₂N⁺), 51.93 ppm (-CH₃), 55.5 ppm (-CH₂OH), 58.36 (bpy⁺-CH₂), 61.06 ppm (CH₂N⁺), 65.40 ppm (-CH₂CH₂OH), 127.51 ppm (-CHCHN⁺ bpy), 145.77 ppm (-CHCHN⁺ bpy), 150.7 ppm (c-quat bpy). ¹⁵N-HMBC (D₂O + TMSP-d₄, Std. CH₃NO₂): -170.8 ppm (N-bipyridine), -329.4 ppm (N-ammonium). HRESI-MS: m/z calculated for C₂₄H₄₂N₄O₂⁴⁺ 104.5822, found 163.6150 [(M⁺ + Br⁻)₃ - 2H⁺], 289.0822 [M⁺/2 + Br⁻ + H⁺]. IR (ATR), (λ^{-1} , cm⁻¹): 3200–3500w, 3000w, 1638 s, 1447s, 1230w. Decomposition point ≈ 265 °C.

Synthesis of 1,1'-bis(3-((2-hydroxyethyl)dimethylammonio)propyl)-[4,4'-bipyridine]-1,1'-dium tetrachloride, [(DMAE-Pr)₂-Vi]Cl₄

1,1'-Bis(3-((2-hydroxyethyl)dimethylammonio)propyl)-[4,4'-bipyridine]-1,1'-dium tetrabromide (7.83 g, 10.6 mmol, 1 equiv.) was dissolved in water and then a solution of NaPF₆ (9.1 g, 54 mmol, 5.1 equiv.) in water was added. The mixture was stirred overnight, filtered using a glass frit and the collected solid washed with water. After drying over high vacuum, the PF₆ salt (10.06 g, 10 mmol, 1 equiv.) was dissolved in acetonitrile and an excess of dried tetrabutylammonium chloride (15 g, 54 mmol, 5.4 equiv.) dissolved in the same solvent was added under strong stirring. The mixture was stirred overnight. (Double metathesis was employed in view of its simplicity when handling concentrated solutions of viologens,^[46] although an ion exchange column can also be used, e.g., Amberlyst IRA-900 resin,^[31] which would eliminate steps and reduce the amount of reagents.) The product was then filtered using a glass frit, washed with hot MeCN and dried (5.4 g, 9.6 mmol, 95% yield). Identical spectroscopic data to the bromide salt (see Figures S7 and S8). The absence of bromine was confirmed by cyclic voltammetry (Figure S11). Molecular weight 560.43 g mol⁻¹. Decomposition point ≈ 250 °C.

DOSY spectroscopy

The sample of [(DMAE-Pr)₂-Vi]Cl₄ was prepared with a concentration of 0.05 M in 1 M KCl D₂O (0.75 wt % of TSMPO-d₄) in a high-quality 3 mm NMR tube (Wilmad 335). Before starting the experiment, the sample was thoroughly degassed through freeze/thaw cycles. All relevant information regarding the applied sequence can be found elsewhere.^[47]

Solubility, viscosity and pH measurements

UV-Vis spectroscopy was used to determine the solubility of [(DMAE-Pr)₂-Vi]Cl₄ by adapting a literature procedure.^[39,48] A calibration curve was built using the absorbance at 260.5 nm (see Figure S9) at concentrations of 2, 4, 10 and 20 μM (see Figure S10), yielding the equation $y = 0.0230x + 0.0016$. Accuracy was confirmed by repeating the procedure with a different salt batch at concentrations of 1, 2, 10 and 15 μM, giving practically identical results ($y = 0.0228x + 0.0009$). Three saturated solutions of the salt were prepared, stirred for 3 days, filtered twice on 0.22 μm PTFE filter and diluted by a factor of 10⁶. The measured absorbance was used to calculate the concentration according to the pre-calibrated absorbance-concentration curve. The value of 2.7 M ± 0.3 (SD) is the average of 6 measurements (2 for each saturated solution). The viscosity of fresh and charged negolyte for the battery was measured by quadruplicate at 25 °C using an Ubbelohde viscosimeter type 501 (SI Analytics) after filtrating the solutions with filter paper. The viscosity of the charged negolyte was measured at the maximum accessible capacity after 1 cycle and immediately after exposure to air. Temperature was controlled within ± 0.5 °C. The pH of the electrolytes was measured with pH-indicator strips (Tritest).

Exploratory cyclic voltammetry and Randles-Ševčík analysis

All the experiments were performed in either 0.1 M or 1 M KCl aqueous solution with an Autolab PGSTAT204 potentiostat/galvanostat (Metrohm). A cell with a three-electrode configuration was used. The glassy carbon working electrode ($d=2$ mm) was polished before each measurement with a 0.03 μm Al₂O₃ slurry and

then rinsed thoroughly with deionized water. A platinum sheet was used as counter electrode, while the reference electrode was Ag/AgCl (3.0 M KCl). The measurements were performed at a temperature of 22 °C under a nitrogen atmosphere after purging the solutions with the same gas for 30 min. Voltammograms were obtained for electrode potential scan rates, ν , between 10 to 1000 mV s⁻¹ (not shown) and between 5 to 5000 mV s⁻¹ (Figure 3b), compensating for IR drop after an EIS scan. Diffusion coefficients, D , were then estimated for the first series of scan rates from the slope of the fitting of peak current density, j_p vs. the square root of ν , according to the Randles-Ševčík equation:

$$j_p = 2.69 \times 10^5 n^{3/2} D^{1/2} c \nu^{1/2} \quad (1)$$

Levich's analysis of diffusion coefficients

The procedure was performed with a concentration of 1 mM in 0.5 M KCl using a WaveVortex 10 electrode rotator (Pine Instruments) and an Interfase 1000 potentiostat/galvanostat (Gamry Instruments). A jacketed glass cell connected to a thermostatic water bath was used in a three-electrode configuration, with a glassy carbon electrode ($d=5$ mm) as working electrode, a platinum gauze as counter electrode and an Ag/AgCl (3.0 M NaCl) reference electrode. The working electrode was polished with 0.05 μm Al₂O₃ slurry before each measurement. Linear sweep voltammetry was carried out at a temperature of 25 °C between electrode potential values of 0.0 V and -1.2 V vs. Ag/AgCl at $\nu = 5$ mV s⁻¹. After deaerating the electrolytes for 30 min, the measurements were performed under a nitrogen atmosphere using a AC01TPA6 M bearing assembly (Pine Instruments). The values of D were calculated from the slope of the linear relationship between limiting current density, j_L , and the square root of rotation rate, $\omega^{1/2}$, in accordance to the Levich equation:

$$j_L = 0.62 n F D^{2/3} c \nu^{-1/6} \omega^{1/2} \quad (2)$$

where n is the number of electrons involved in the reaction, F is the Faraday constant, c is the concentration of the species in solution and ν is the kinematic viscosity of the solution, which is 0.0088 cm² s⁻¹ for 0.5 M KCl.^[30,48] The reported values are the arithmetic average of triplicate measurements. j_L values were corrected for background electrolyte current.

Flow battery experiments

Battery performance data were collected in a 4 cm² LabCell (Pinflow) connected to an Interface 5000E potentiostat-galvanostat (Gamry Instruments) in two-electrode mode. The electrodes were 4.6 mm thick Sigracell GDF 4,6 EA carbon felt (SGL Carbon) activated for 30 h at 400 °C under air.^[49] After assembling the rectangular channel flow cell and tightening its bolts with a torque of 8 N m each, the felts acquired a thickness of 4.0 mm, hence compressed to approximately 87% of their original thickness. Anion exchange FAS-30 (Fumatech) with a nominal thickness of 30 μm was used after being immersed in the supporting electrolyte for at least 24 h. The flow system comprised a Masterflex Drive L/S® 600R peristaltic pump (Cole-Parmer) employing Viton® and FEP tubing. Glass vials within 100 mL amber glass bottles with Viton-sealed multiport HPLC caps (Bola) were used as electrolyte reservoirs and purged with humidified nitrogen for 1 h prior to the experiments. Additionally, all exposed sections of the flow system were covered from ambient light. Electrolyte flow rate was set to 43.7 mL min⁻¹ (50 rpm), equivalent to an average linear velocity of

$\approx 1.0 \text{ cm s}^{-1}$ through each electrode. For a starting concentration of 0.1 M active species, this flow rate represents a stoichiometric factor (S) of 43.9 at a constant current density of 40 mA cm^{-2} in this cell. Experiments were carried out at a temperature of approximately 22°C .

DFT Calculations

First, the structures for the cations BTMAP-Vi, BHOE-Vi BHOP and for the new cation $(\text{DMAE-Pr})_2$ were optimized by XTB^[50] and a conformer ensemble was created for each cation with CREST.^[51,52] The conformer with the highest Boltzmann weight was determined by CENSO^[53] for each cation. Each conformer with the highest Boltzmann weight was further optimized with ORCA^[54,55] using the functional B3LYP with a dispersion correction^[56,57] and the common basis set def2-TZVP.^[58] For the solvent, water was used with the COSMO model. The analytical frequency calculations of each optimized structure showed no negative vibrations. The HOMO/LUMO-levels for each optimized structure was thereafter also calculated single point by using the SMD solvent model. For the cation $(\text{DMAE-Pr})_2$ the procedure was repeated for each of its oxidation states. The reported HOMO/LUMO level are from the calculations with the SMD model.

Acknowledgements

LFA is grateful to the Alexander von Humboldt Foundation (Germany) for sponsoring a fellowship at TU Clausthal and thanks Dr. Oliver Rodríguez for fruitful discussions and Mr. Lavrans Söfftker for evaluating electrolyte viscosity. Dr. Jan C. Namyslo is acknowledged for DOSY measurements. Open Access funding enabled and organized by Projekt DEAL.

Conflict of Interest

The authors declare no conflict of interest.

Data Availability Statement

The data that support the findings of this study are available in the Supporting Information of this article.

Keywords: density functional calculations • electrochemistry • energy storage • redox flow battery • viologen

- [1] L. F. Arenas, J. J. H. Pijpers, in *Encyclopedia of Energy Storage*, Vol. 2 (Ed.: L. F. Cabeza), Elsevier, Oxford, 2021, pp. 524–534.
- [2] J. Girschkik, L. Kopietz, M. Joemann, A. Grevé, C. Doetsch, *Chem. Ing. Tech.* 2021, 93, 523–533.
- [3] E. Sánchez-Díez, E. Ventosa, M. Guarnieri, A. Trovò, C. Flox, R. Marcilla, F. Soavi, P. Mazur, E. Aranzabe, R. Ferret, *J. Power Sources* 2021, 481, 228804.
- [4] P. Leung, A. A. Shah, L. Sanz, C. Flox, J. R. Morante, Q. Xu, M. R. Mohamed, C. Ponce de León, F. C. Walsh, *J. Power Sources* 2017, 360, 243–283.
- [5] V. Singh, S. Kim, J. Kang, H. R. Byon, *Nano Res.* 2019, 12, 1988–2001.
- [6] C. Wang, X. Li, B. Yu, Y. Wang, Z. Yang, H. Wang, H. Lin, J. Ma, G. Li, Z. Jin, *ACS Energy Lett.* 2020, 5, 411–417.
- [7] S. R. Narayan, A. Nirmalchandar, A. Murali, B. Yang, L. Hooper-Burkhardt, S. Krishnamoorthy, G. K. S. Prakash, *Curr. Opin. Electrochem.* 2019, 18, 72–80.
- [8] D. G. Kwabi, Y. Ji, M. J. Aziz, *Chem. Rev.* 2020, 120, 6467–6489.
- [9] L. Striepe, T. Baumgartner, *Eur. J. Chem.* 2017, 23, 16924–16940.
- [10] S. Muench, A. Wild, C. Fribe, B. Häupler, T. Janoschka, U. S. Schubert, *Chem. Rev.* 2016, 116, 9438–9484.
- [11] P. Monk, R. Mortimer, D. Rosseinsky, in *Electrochromism and Electrochromic Devices*, Cambridge University Press, Cambridge, 2007, pp. 341–373.
- [12] K. Madasamy, D. Velayutham, V. Suryanarayanan, M. Kathiresan, K.-C. Ho, *J. Mater. Chem. C* 2019, 7, 4622–4637.
- [13] S.-S. Jang, S.-K. Park, S.-H. Yeon, K.-H. Shin, H. Song, H.-S. Kim, Y.-S. Jung, C.-S. Jin, *J. Electrochem. Soc.* 2021, 168, 100532.
- [14] T. Janoschka, N. Martin, M. D. Hager, U. S. Schubert, *Angew. Chem. Int. Ed.* 2016, 55, 14427–14430; *Angew. Chem.* 2016, 128, 14639–14643.
- [15] Z. Burešová, M. Klikar, P. Mazúr, M. Mikešová, J. Kvíčala, T. Bystron, F. Bureš, *Front. Chem.* 2021, 8, 1289.
- [16] E. S. Beh, D. De Porcellinis, R. L. Gracia, K. T. Xia, R. G. Gordon, M. J. Aziz, *ACS Energy Lett.* 2017, 2, 639–644.
- [17] S. Jin, E. M. Fell, L. Vina-Lopez, Y. Jing, P. W. Michalak, R. G. Gordon, M. J. Aziz, *Adv. Energy Mater.* 2020, 10, 2000100.
- [18] C. DeBruler, B. Hu, J. Moss, J. Luo, T. L. Liu, *ACS Energy Lett.* 2018, 3, 663–668.
- [19] C. DeBruler, B. Hu, J. Moss, X. Liu, J. Luo, Y. Sun, T. L. Liu, *Chem* 2017, 3, 961–978.
- [20] M.-A. Goulet, M. J. Aziz, *J. Electrochem. Soc.* 2018, 165, A1466–A1477.
- [21] B. Hu, Y. Tang, J. Luo, G. Grove, Y. Guo, T. L. Liu, *Chem. Commun.* 2018, 54, 6871–6874.
- [22] Y. Liu, Y. Li, P. Zuo, Q. Chen, G. Tang, P. Sun, Z. Yang, T. Xu, *ChemSusChem* 2020, 13, 2245–2249.
- [23] G. Tang, Y. Liu, Y. Li, K. Peng, P. Zuo, Z. Yang, T. Xu, *JACS Au* 2022, 2, 1214–1222.
- [24] X.-L. Lv, P. Sullivan, H.-C. Fu, X. Hu, H. Liu, S. Jin, W. Li, D. Feng, *ACS Energy Lett.* 2022, 7, 2428–2434.
- [25] L. Liu, Y. Yao, Z. Wang, Y.-C. Lu, *Nano Energy* 2021, 84, 105897.
- [26] H. Wang, S. Y. Sayed, E. J. Luber, B. C. Olsen, S. M. Shirurkar, S. Venkatakrishnan, U. M. Tefashe, A. K. Farquhar, E. S. Smotkin, R. L. McCreery, J. M. Buriak, *ACS Nano* 2020, 14, 2575–2584.
- [27] E. Martínez-González, M. M. Flores-Leonar, C. Amador-Bedolla, V. M. Ugalde-Saldívar, *ACS Appl. Energ. Mater.* 2021, 4, 6624–6634.
- [28] J. E. Nolan, J. A. Plambeck, *J. Electroanal. Chem.* 1990, 294, 1–20.
- [29] C.-W. Lee, L. J. C. Eklund, R. A. W. Dryfe, R. G. Compton, *Bull. Korean Chem. Soc.* 1996, 17, 162–167.
- [30] B. Hu, C. Seefeldt, C. DeBruler, T. L. Liu, *J. Mater. Chem. A* 2017, 5, 22137–22145.
- [31] G. Tang, Y. Liu, Y. Li, K. Peng, P. Zuo, Z. Yang, T. Xu, *JACS Au* 2022, 2, 1214–1222.
- [32] T. Hagemann, J. Winsberg, M. Grube, I. Nischang, T. Janoschka, N. Martin, M. D. Hager, U. S. Schubert, *J. Power Sources* 2018, 378, 546–554.
- [33] J. Luo, B. Hu, C. Debruler, T. L. Liu, *Angew. Chem. Int. Ed.* 2018, 57, 231–235; *Angew. Chem.* 2018, 130, 237–241.
- [34] T. Lemmermann, M. Becker, M. Stehle, M. Drache, S. Beuermann, M. S. Bogar, U. Gohs, U. E. A. Fittschen, T. Turek, U. Kunz, *J. Power Sources* 2022, 533, 231343.
- [35] S. Hu, T. Li, M. Huang, J. Huang, W. Li, L. Wang, Z. Chen, Z. Fu, X. Li, Z. Liang, *J. Adv. Mater.* 2021, 33, 2005839.
- [36] H. Wang, D. Li, J. Xu, Y. Wu, Y. Cui, L. Chen, *J. Power Sources* 2021, 492, 229659.
- [37] J. R. Thurston, S. E. Waters, B. H. Robb, M. P. Marshak, in *Encyclopedia of Energy Storage* (Ed.: L. F. Cabeza), Elsevier, Oxford, 2022, pp. 423–435.
- [38] B. Hu, C. DeBruler, Z. Rhodes, T. L. Liu, *J. Am. Chem. Soc.* 2017, 139, 1207–1214.
- [39] Y. Liu, M.-A. Goulet, L. Tong, Y. Liu, Y. Ji, L. Wu, R. G. Gordon, M. J. Aziz, Z. Yang, T. Xu, *Chem* 2019, 5, 1861–1870.
- [40] B. Liu, C. W. Tang, H. Jiang, G. Jia, T. Zhao, *J. Power Sources* 2020, 477, 228985.
- [41] L. Wylie, T. Blesch, R. Freeman, K. Hatakeyama-Sato, K. Oyaizu, M. Yoshizawa-Fujita, E. I. Izgorodina, *ACS Sustainable Chem. Eng.* 2020, 8, 17988–17996.
- [42] Y. Liu, Q. Chen, X. Zhang, J. Ran, X. Han, Z. Yang, T. Xu, *Curr. Opin. Electrochem.* 2022, 32, 100895.

- [43] X. Lv, P. Sullivan, W. Li, H.-C. Fu, R. Jacobs, C.-J. Chen, D. Morgan, S. Jin, D. Feng, *ChemRxiv*. 2022, <https://doi.org/10.26434/chemrxiv-2022-hpktf>.
- [44] A. M. Fenton, R. K. Jha, B. J. Neyhouse, A. P. Kaur, D. A. Dailey, S. A. Odom, F. R. Brushett, *J. Mater. Chem. A* 2022, 10, 17988–17999.
- [45] P. Ochtrup, S. Ernst, A. Itzen, C. Hedberg, *ChemBioChem* 2019, 20, 2336–2340.
- [46] X. Tang, T. W. Schneider, J. W. Walker, D. A. Buttry, *Langmuir* 1996, 12, 5921–5933.
- [47] J. C. Namyslo, M. H. H. Drafz, D. E. Kaufmann, *Polymer* 2021, 13, 2164.
- [48] S. Hu, L. Wang, X. Yuan, Z. Xiang, M. Huang, P. Luo, Y. Liu, Z. Fu, Z. Liang, *Energy Mater. Adv.* 2021, 2021, 1–8.
- [49] B. Sun, M. Skyllas-Kazacos, *Electrochim. Acta* 1992, 37, 1253–1260.
- [50] C. Bannwarth, E. Caldeweyher, S. Ehlert, A. Hansen, P. Pracht, J. Seibert, S. Spicher, S. Grimme, *WIREs Comput. Mol. Sci.* 2021, 11, e1493.
- [51] P. Pracht, F. Bohle, S. Grimme, *Phys. Chem. Chem. Phys.* 2020, 22, 7169–7192.
- [52] S. Grimme, *J. Chem. Theory Comput.* 2019, 15, 2847–2862.
- [53] S. Grimme, F. Bohle, A. Hansen, P. Pracht, S. Spicher, M. Stahn, *J. Phys. Chem. A* 2021, 125, 4039–4054.
- [54] F. Neese, *WIREs Comput. Mol. Sci.* 2012, 2, 73–78.
- [55] F. Neese, *WIREs Comput. Mol. Sci.* 2018, 8, e1327.
- [56] S. Grimme, J. Antony, S. Ehrlich, H. Krieg, *Chem. Phys.* 2010, 132, 154104.
- [57] S. Grimme, S. Ehrlich, L. Goerigk, *J. Comput. Chem.* 2011, 32, 1456–1465.
- [58] F. Weigend, R. Ahlrichs, *Phys. Chem. Chem. Phys.* 2005, 7, 3297.

Manuscript received: August 11, 2022

Revised manuscript received: September 19, 2022

Accepted manuscript online: October 3, 2022

Version of record online: October 26, 2022